Applied Catalysis B: Environmental 142–143 (2013) 736–743

Contents lists available at SciVerse ScienceDirect

Applied Catalysis B: Environmental

journal homepage: www.elsevier.com/locate/apcatb

# Defect and its dominance in ZnO films: A new insight into the role of defect over photocatalytic activity

Zengxia Pei, Luyao Ding, Jun Hu, Sunxian Weng, Zuyang Zheng, Mianli Huang, Ping Liu*

*State Key Laboratory Breeding Base of Photocatalysis, Research Institute of Photocatalysis, Fuzhou University, Fuzhou 350002, PR China*

ARTICLE INFO

*Article history:*
Received 21 February 2013
Received in revised form 8 May 2013
Accepted 22 May 2013
Available online 29 May 2013

*Keywords:*
ZnO
Defect
Photocatalysis

ABSTRACT

Influence of defect on photocatalyst is in extensive concern. In the present contribution, by cold plasma treatment (CPT) technique and dip-coating method, we successfully prepared ZnO bilayer films with oxygen vacancies and interstitial zinc atoms. The defective films showed promoted photocatalytic activity, with enhanced transportation and good separation of photogenerated charge carriers being the main reasons. More importantly, combination of CPT and dip coating method allowed us to investigate the dominance of defect and its stability. Our work may not only provide helpful information for better understanding of relationship between defect and photocatalysis, but also offer a new strategy for designing stabilized defect-modulated photocatalyst.



## 1. Introduction

Due to its various applications in piezoelectric [1], optical [2], electronic [3], catalytic [4] and photocatalytic [5–8] areas, ZnO has been widely investigated in recent years. Among its varied functions, photocatalytic performance of ZnO is in extensive concern since this semiconductor, as a photocatalyst, has been used for environmental remediation [6–8] and clean energy production [9,10]. Sharing the similarities with $TiO_2$, another well-known photocatalyst, in nontoxic, nature and low cost, ZnO is always believed to be an alternative promising photocatalytic material [7,9]. Recent researches [7,11] showed that ZnO exhibits better activity in some cases in contrast with $TiO_2$ as a result of the former's higher mobility of charge carriers. Even so, the photoreactivity of ZnO is still not that satisfying and further modification is indeed needed.

Among various methods [12–15] that have been developed to enhance the photoreactivity of ZnO, much attentions are paid to defect-related photocatalytic performance of ZnO since long have been the controversy on the effect of defect over photocatalytic activity [7,11,15,16] and defect is of intrinsic ubiquity in the material [16,17]. Some researches [7,11,16] indicate that lower defect concentration has beneficial effect while other studies [15,18] report that increased defect accounts for the improved photoreactivity. However, it is generally accepted that surface defects act as trapping centers thus facilitate photoinduced charge carriers' separation whereas bulk ones only serve as recombination sites [19–21]. Recently, Kong et al. [20] revealed by positron annihilation that tuning the relative concentration ratio of bulk defects to surface defects in $TiO_2$ leads to high photocatalytic efficiency. In distinct contrast with surface/bulk defects, those in the subsurface, or probably could be called interface, are not that much investigated [19,22].

Generally, defects located at the outermost layer will directly contact with reactants which could contaminate the active sites hence deactivates the catalyst [23]. In addition, exposure of surface defects in circumstance makes these defects easily repaired [19,24] by oxygen and/or other oxidative species. In the very recent, researchers [25,26] have succeeded in preparing black $TiO_2$ with defective core/shell structure and this photocatalyst shows quite long stability. Their works imply that intimal defects could, to some extent, affect the photocatalytic process and that long stabilization of defects is possible. Now that defect can indeed boost the photocatalytic efficiency, then the question naturally occurs: where is the dominance of defect and how to evaluate its role?

Traditional methods like hydrogen reduction [26,27], high temperature calcination [28] and particle bombardment [29] can create defects both in the surface and bulk. The random distribution adds difficulty to study of defect. Besides, farinose photocatalyst may have different specific surface and is hard to reproduce. All these drawbacks hinder the investigation concerning defect. CPT technology is an effective technique which can only create defects on metal oxide surface at low temperature without changing the bulk properties and had been demonstrated in our previous work [19,22]. Film has advantages like reproducible and controllable properties including thickness, microstructure and surface morphology. In the present work, different defective ZnO bilayer films were

* Corresponding author. Tel.: +86 591 8377 9239; fax: +86 591 8377 9239.
*E-mail address:* liuping@fzu.edu.cn (P. Liu).

0926-3373/$ – see front matter © 2013 Elsevier B.V. All rights reserved.
http://dx.doi.org/10.1016/j.apcatb.2013.05.055

successfully prepared by CPT technique together with dip coating method. By changing the thickness of the outer layer, we were able to study the dominance scope of defect. Choosing methyl orange (MO) and 4-chlorophenol (4-CP) as typical toxic industrial effluents and reducing 4-nitrianiline (4-NA) to p-phenylenediamine (PPD) as model reactions, the role of defect in both photocatalytic oxidation and reduction is also traversed. We believe that the present work may provide a new insight into the role of defect in certain positions over photocatalytic activity.

## 2. Experimental

### 2.1. Materials

Zinc oxide colloidal dispersion (40% in $H_2O$) was purchased from Alfa Aesar. Methyl orange (MO), 4-chlorophenol (4-CP), 4-nitrianiline (4-NA), terephthalic acid (TA), methanol, isopropanol, sodium hydroxide and $H_2O_2$ were all obtained from Sinopharm Chemical Reagent Co. Ltd., and all of these reagents were analytical pure and used without further purification. Deionized water was used throughout the work.

### 2.2. Preparation of ZnO films with/without defect

The ZnO layers were deposited onto clean quartz slides (25 mm × 75 mm × 1 mm) by dip coating the diluted ZnO colloidal with the ratio $H_2O$:ZnO = 2:1 (v/v) at certain drawing rate under ambient circumstance. Schematics can be found in Supporting Information (Figure S1). In a typical sample preparation, the first layer was drawn at the rate of 20 mm/min and calcined at 473 K for 30 min. Then the monolayer sample was transferred to a previously He flushed quartz vacuum chamber and treated with cold plasma discharge (450 W) for 5 min in rarefied He atmosphere. After that, the film was again immersed into the dispersion to be coated with another ZnO layer via repeating the coating and drying process. Hereto, a bilayer film with defect between the layers was prepared and marked as interface defective ZnO (Z-ID). To contrast with this, a normal surface film was prepared exactly as the Z-ID one's procedure except being free of CPT and was denoted as Z-NS. Moreover, a surface defective (Z-SD) sample was also prepared by CPT over the surface of Z-NS one. For the study of dominance of defective sites, drawing rates of the second layers of Z-NS & Z-ID ones varied every 20 mm/min from 20 mm/min to 100 mm/min with other conditions remained unchanged.

### 2.3. Characterization

Crystal structure identification was performed using Bruker D8 X-ray diffractometer (XRD) with Cu Kα radiation operating at 40 kV and 40 mA. The ZnO bilayer film was too thin to got a fine XRD pattern so the coating time increased to 5. Energy Dispersive X-ray Spectroscopy (EDX) investigation was carried out on an FEI Nova NanoSEM 230 field-emission scanning electron microscope. Microstructures and morphologies were investigated using TecnaiG2 F20 S-TWIN (FEI company) Transmission electron microscopy (TEM) with a field emission gun at 200 kV. For observation of surface roughness, atomic force microscopy (AFM, Nanoscope Multimode IIIa microscope, Veeco Instrument) was used. The root-mean-square roughness values ($R_{rms}$) were estimated by spectral analysis on 1 μm$^2$ areas. X-ray photoelectron spectroscopy (XPS) analysis was conducted on an ESCALAB 250 photoelectron spectroscopy (Thermo Fisher Scientific) at $1.2 \times 10^{-9}$ mbar using Al Kα X-ray beam (1486.6 eV). A Bruker model A300 spectrometer was used for detection of the electron-spin resonance (ESR) signals of samples at room temperature. Diffuse reflection spectra (DRS) of the samples were recorded on a Varian Cary-500 spectrophotometer. UV–vis spectra were measured on a UV–vis–NIR spectrometer (Cary-500). For the characterization of EDX, TEM and ESR, the powders used were carefully scratched off the ZnO films before test.

### 2.4. Photocatalytic activity test

The photocatalytic activity of the ZnO films was estimated by both photodegradation and selective reduction. For the decomposition section, MO and 4-CP were elected as model contaminants with a concentration of $3 \times 10^{-5}$ M and $10^{-4}$ M, respectively. 4-NA, with a 5 mg/L concentration, was reduced with addition of 500 μL methanol as photo-generated hole scavenger and the whole photocatalytic process was carried out under $N_2$ bubbling with a flow rate of 60 mL/min. For all reactions, 2 pieces of slides were immersed into 50 mL of each solution in a quartz tube. Four UV lamps (4 W, Philips TL/05) surrounded the tube reactor and provide illumination with a predominant wavelength at 365 nm (5 mW/cm$^2$). Prior to irradiation, stir in dark for 30 min was allowed for establishment of adsorption/desorption equilibrium. Change in absorbance of the solution was used to monitor the extent of photocatalytic reaction. At given irradiation time intervals, 3 mL of the solution was taken out and quickly analyzed on the UV–vis spectrometer. After every assay, the analyzed liquid was poured back into the reaction system to ensure a constant volume of the solution. The final efficiency was calculated by the following equation:

$$E_t(\%) = \left(1 - \frac{C_t}{C_0}\right) \times 100\%,$$

where $C_0$ and $C_t$ stands for the initial and final concentration of reactants, respectively.

### 2.5. Photoelectrochemical measurements

Photoelectrochemical tests were conducted on a ZENNIUM electrochemical workstation (Zahner, Germany) with conventional three-electrode method. The FTO/NS and FTO/ID ZnO film electrodes served as the working electrode. The counter and reference electrodes were Pt plate and Ag/AgCl electrode and 0.2 M $Na_2SO_4$ (pH = 6.8) served as electrolyte. For Electrochemical impedance spectra (EIS) tests, a 300 W xenon lamp was used to provide UV light source with an optical filter (365 ± 15 nm). The amplitude of the sinusoidal wave was 10 mV, and the frequency range of the sinusoidal wave was from 4 MHz to 0.01 Hz. The Mott–Schottky plots to determine the flat-band potential ($U_{fb}$) of the semiconductor space charge region was obtained by measuring impedance spectra at fixed frequency of 1 kHz in dark.

## 3. Results and discussion

### 3.1. Size and crystal structure of ZnO on the film

XRD patterns of ZnO on the films are shown in Fig. 1. Three major peaks are observed at $2\theta \approx 31.8^\circ$, $34.5^\circ$ and $36.3^\circ$, which can be assigned to (1 0 0), (0 0 2) and (1 0 1) lattice planes, respectively. These diffraction peaks are well indexed to hexagonal ZnO wurtzite structure (JCPDS 75-0576). It is worth noting that despite the CPT process, diffraction patterns of the SD film match quite well with those of the NS one. This proves that CPT is just a surface-treatment technique and does not make any difference on the crystal phase and size. From TEM observations it is further revealed that ZnO crystals consist of particles of different sizes and shapes, with an average size of 30 nm as shown in Fig. 2(A). HRTEM image of Fig. 2(B) clearly indicates typical ZnO nanoparticles with lattice fringes of $d$ = 0.248 nm that are well matched with the crystallographic planes of wurtzite (1 0 1). Shown in Fig. 3 are the surface images of ZnO film

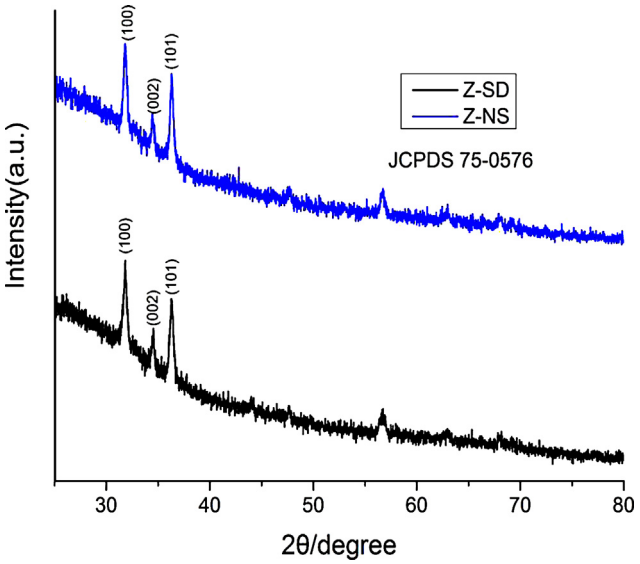


**Fig. 1.** XRD patterns of as-prepared ZnO films.

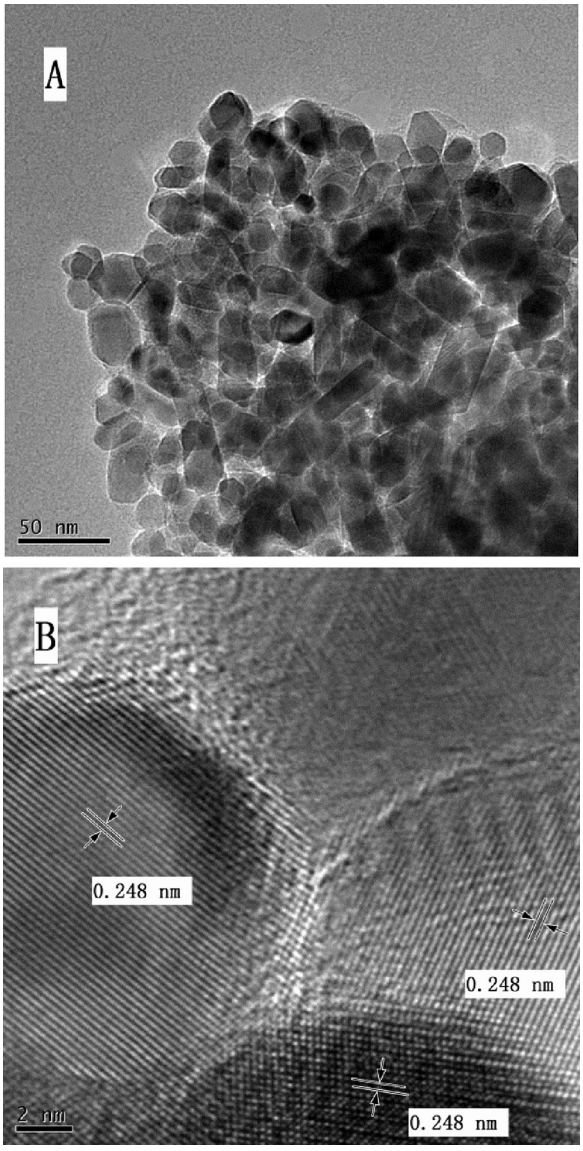


**Fig. 2.** (A) TEM and (B) HRTEM images of ZnO particles.

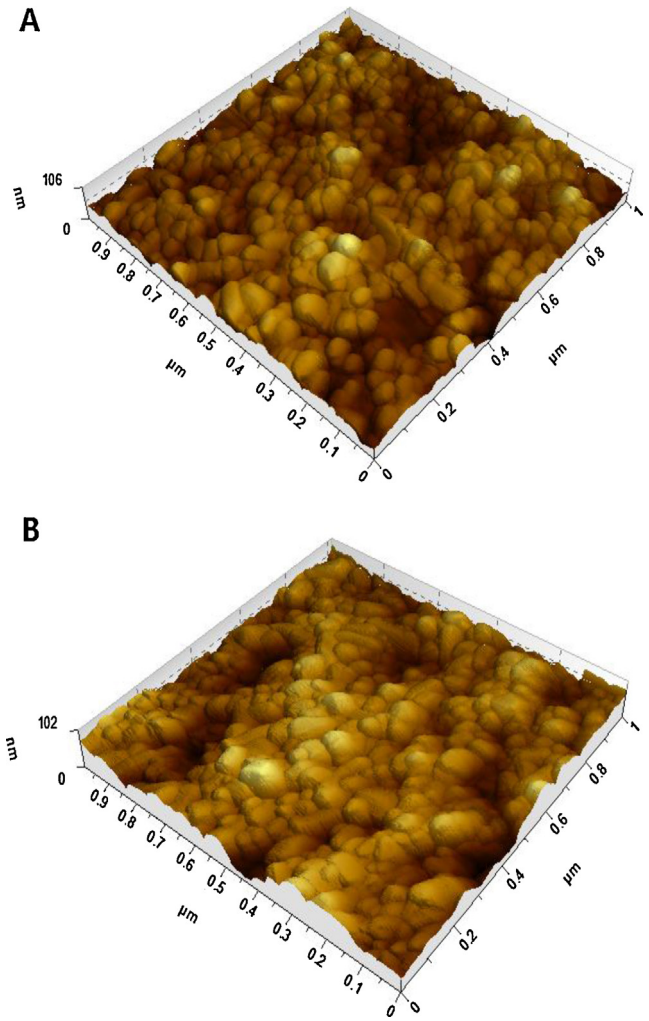


**Fig. 3.** Three-dimensional AFM images of the ZnO film surface before (A) and after (B) CPT.

before (A) and after (B) CPT. The results of AFM demonstrate the surface morphology and particle size remained almost unchanged during CPT process. Besides, the surface roughness states are also similar despite cold plasma treatment, as the $R_{rms}$ values of the film before and after CPT is 13.6 nm and 14.1 nm, respectively. Results from XRD, TEM and AFM analysis confirm that no extrinsic properties like size, specific surface area and special morphology or surface roughness account for the differences of photocatalytic activity which will be discussed in the following.

### 3.2. Surface state of the as-prepared ZnO films

To truly illustrate the surface composition and chemical state of ZnO, XPS measurements were conducted on films directly. Both NS and SD films were investigated because XPS is a very powerful technique to detect surface [30–33]. As shown in Fig. 4, O 1s core level spectra are quite asymmetric with a broad shoulder by the side of higher binding energy, which manifests rich oxygen states on the surface. The spectra of SD film can be best fitted into 3 peaks while the NS one has 4 curves. Main peak at about $530.1 \pm 0.1$ eV is attributed to oxygen in the ZnO crystal lattice ($O_L$) [31,33]. The higher binding energy ($O_H$) at some $532.0 \pm 0.1$ eV relates to hydroxyl groups [32]. A medium binding energy component, centered at $531.3 \pm 0.2$ eV, is generally associated with $O^{2-}$ ions in the oxygen deficient regions ($O_D$) within the matrix of ZnO [31,33]. An even higher peak, shown in NS film only, located at

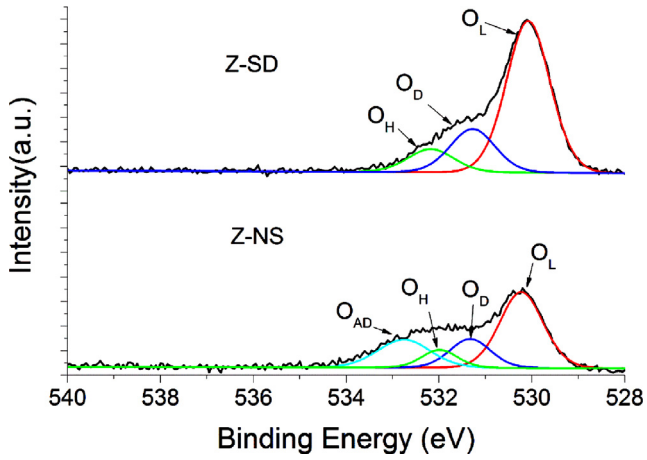


**Fig. 4.** XPS O 1s spectra of SD and NS ZnO films.

532.7 ± 0.2 eV, can be attributed to chemisorbed or dissociated oxygen species ($O_{AD}$) on the surface of ZnO film, such as adsorbed $H_2O$ and/or $O_2$ [31,33]. Asymmetric Zn 2p XPS spectra without notable difference except relative intensity can be found in Figure S2. The asymmetry in both spectra denotes that interstitial zinc ($Zn_i$) atoms may exist [30,31]. Something significant to note here is the increase of $O_D$ (13.2–16.3%) and $O_H$ (10.4–15.6%), together with remarkable decrease of $O_{AD}$ (23.4–0) comparing results of NS film to SD film's. It goes without saying that $O_D$s lie around defective sites. Moreover, $O_H$ atoms are probably resulting from dissociated $H_2O$ on surface defects (e.g., oxygen vacancies) [19,34]. Thus, both higher $O_D$ and $O_H$ contents mean more defects on the SD film. According to the rules of quantitative analysis of XPS spectrum as following,

$$\frac{n(E_1)}{n(E_2)} = \frac{[A(E_1)/S(E_1)]}{[A(E_2)/S(E_2)]}$$

(where $n$ is the atomic ratio, $A$ represents the area of peak, $E$ is the element and $S$ represents the sensitivity factor of element), the ratio of Zn atoms to the lattice $O^{2-}$ ions ($O_L$ and $O_D$) is 1.07 and 1.21 for NS and SD ZnO samples respectively. It is no surprising that ZnO nanocrystal has non-stoichiometric atom ratio since this material is known to have abundant native defects [16]. XPS observations here demonstrate that CPT can further create more defective sites on ZnO surface. Adsorbed molecules ($O_{AD}$) are probably etched by plasma and then pumped out from a vacuum chamber.

### 3.3. Photocatalytic measurements

#### 3.3.1. Photodegradation tests

*3.3.1.1. Photooxidation of MO and 4-CP.* For clarifying the role of defects and its location in photoreactivity, we first compared the activity of different films in photodecomposition of MO. As can be seen in Fig. 5(A), no observable change of absorbance of MO was detected without photocatalyst, labeled by blank, under 365 nm irradiation after 180 min. In contrast, 58% of the stable azo dye was degraded in the presence of NS ZnO films. Moreover, 87% of MO molecules were decomposed during 3 h by ID ZnO while the ratio reached 92% for SD ones within only 135 min. Photodegradation of dye follows pseudo-first-order kinetics, as confirmed in Fig. 5(B), by linear transforms $\ln(C_0/C) = kt$, where $C_0$ is the adsorption equilibrium concentration of MO, $C$ is the concentration at given interval time. The rate constant are 1.07 $h^{-1}$ and 0.57 $h^{-1}$ for SD and ID film separately, which is 4.3 and 2.3 times higher than that of the NS one (0.25 $h^{-1}$).

While the treatment of azo dye wastewater remains a difficult problem at present, phenols are even more toxic, stable yet

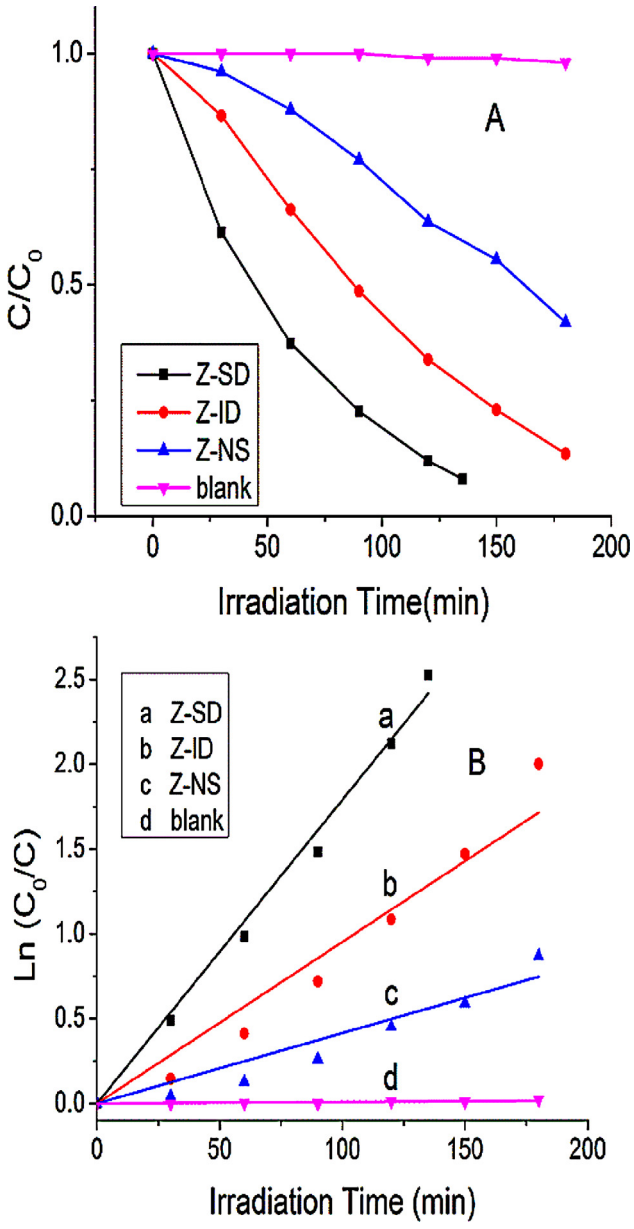


**Fig. 5.** Photodegradation of MO by different ZnO films under UV light irradiation: (A) variations of concentration of MO during degradation process; (B) fitting results using pseudo-first-order kinetics.

widespread in effluents [11]. To further confirm the photooxidation capacity of ZnO, 4-CP was used as another target pollutant and the results are displayed in Fig. 6. After 5 h of illumination, the above-mentioned ZnO samples showed similar decomposition style and efficiency according to the absorbance change at 225 nm. Here again, defective ZnO films still showed excellent activity.

*3.3.1.2. Primary reactive oxidative species (ROS) in decomposition process.* In principle, degradation of pollutants can occur via either direct oxidation by photogenerated holes or reaction with generated intermediate oxygen species [16,22,35]. It is interesting yet important to determine the active species involved in the present systems. To elucidate the role of main ROS, degradation of MO was carried out with different scavengers.

Isopropanol has been described as the best hydroxyl radical quencher and is widely used to distinguish oxidation by hole or by $^{\bullet}OH$ [22,36]. Fig. 7(A) shows the response of photooxidation of MO

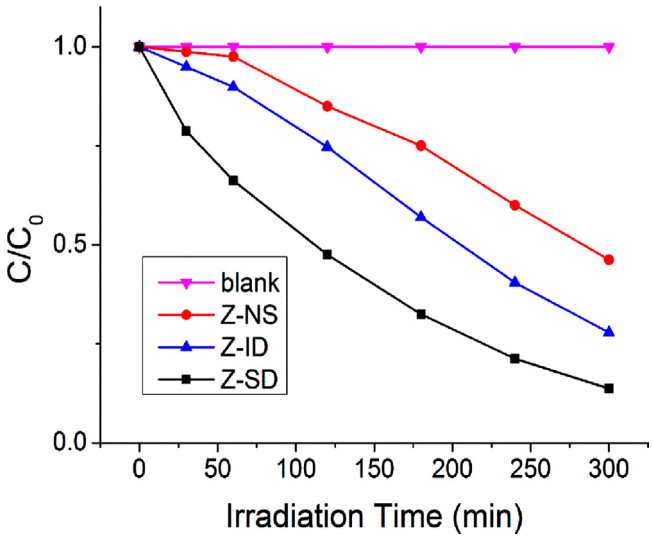


**Fig. 6.** Concentration changes of 4-CP within 5 h under UV light irradiation.

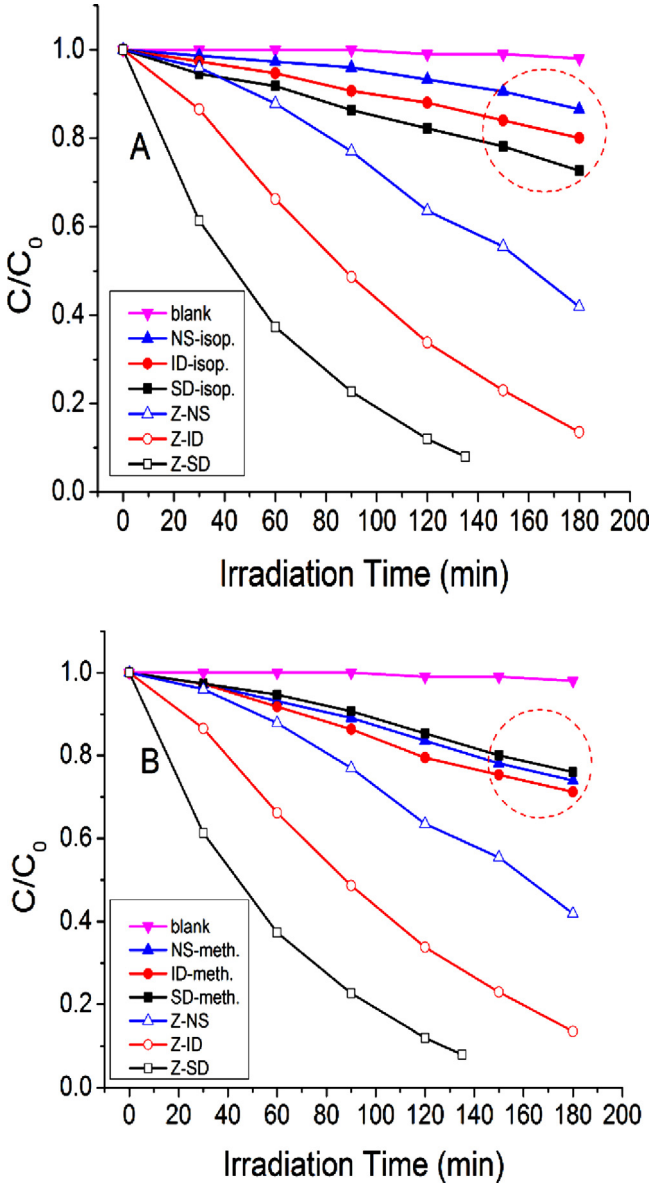


**Fig. 7.** Effects of different scavenger addition in the photocatalyzed degradation of MO: (A) isopropanol, 500 μL; (B) methanol, 500 μL.

after addition of 500 μL isopropanol. Great inhibition was observed in all systems and only small quantity of MO was eliminated by each ZnO film pairs. This result strongly reveals that •OH plays essential role in present experiments. In this way, the higher reactivity of defective zinc oxide films over the NS one is probably due to their higher capability to generate hydroxyl radicals. To further verify this speculation, we used TA to capture •OH and then compared the fluorescence intensity of the product with certain wavelength excitation [35] (see Figure S3). At same time interval, all of the luminescent intensity conformed to the order SD > ID > NS, suggesting a diminishing hydroxyl radical concentration. The semi-quantitative result agrees quite well with our postulation.

It was generally accepted that [37] hydroxyl radicals are generated via two routes: electron-transfer mediation and the photogenerated holes reaction. Then where does •OH originate from in the present experiment? To make clear this issue, methanol, as an efficient hole scavenger [38], was added into the solution before illumination. Fig. 7(B) displays the results of time-dependent degradation process. Again, extensive suppression was observed. The UV–vis spectrogram illustrates that hydroxyl radical are predominately generated by holes. It is interesting to note that efficiency of SD ZnO deteriorates more after addition of methanol, as circled in both figures, in contrast with ID and NS ones. Reason accounting for this phenomenon is that defects on the surface are more easily affected by reaction medium. Besides, decomposition of MO is more dependent on photogenerated holes because of the close contact as a consequence of Coulomb attraction between anionic dye and positive surface with oxygen vacancy. Here, defects on interface show their superiority. We deduce the situation may be quite similar in ZnO/4-CP systems.

### 3.3.2. *Reduction of 4-NA*

Transformation of nitro organics always couples with massive wastewater, offscum and harsh reaction conditions, together with high cost and tedious procedures by conventional techniques [39–41]. Thus, development of new process for transformation of organic compounds is an important goal for chemists pursuing environmentally “green” chemistry. PPD, as one of the simplest aromatic diamines, is a poisonous yet quite significant intermediate in many industries. Recently, photoreduction of 4-NA to PPD has drawn much attentions [39,40]. Herein, we look into the activity of ZnO samples with a simple method provided by Wu et al. [39]. Fig. 8(A) shows the typical evolution of the UV–vis spectral during photoreduction of 4-NA over SD ZnO films under 365 nm. Absorption peaks at 380 nm and 238 nm are characteristic peaks of 4-NA and PPD, respectively. As illustrated in Fig. 8(B), defective ZnO samples show better performance than that of NS one. Time needed to reach a similar conversion quantity around 0.7 is 2 h and 3 h for SD and ID films, both of which are shorter compared with NS's (4 h).

Different films showed distinct performance and defect seemed to be the cause. At present, mechanism of photocatalytic reduction of nitro organics is still disputable [39–41]. Wu et al. [40] reported that α-hydroxyalkyl radicals generated from alcoholic donors (by oxidation) act as main reducing agent. In other words, holes and/or derived hydroxyl radicals oxidize alcohols and then the generated α-hydroxyalkyl radicals play the role of primary reducing species. However, other research [41] indicated that conduction band electrons are mainly responsible for nitro organic reduction. In the present experiment, we believe that no matter which mechanism involved, highly separation of photo-generated charge carriers may play vital role in the enhanced reduction efficiency. By either direct electron reduction or indirect oxidation (α-hydroxyalkyl radical route), or both, separated electron and hole will facilitate the final reduction.

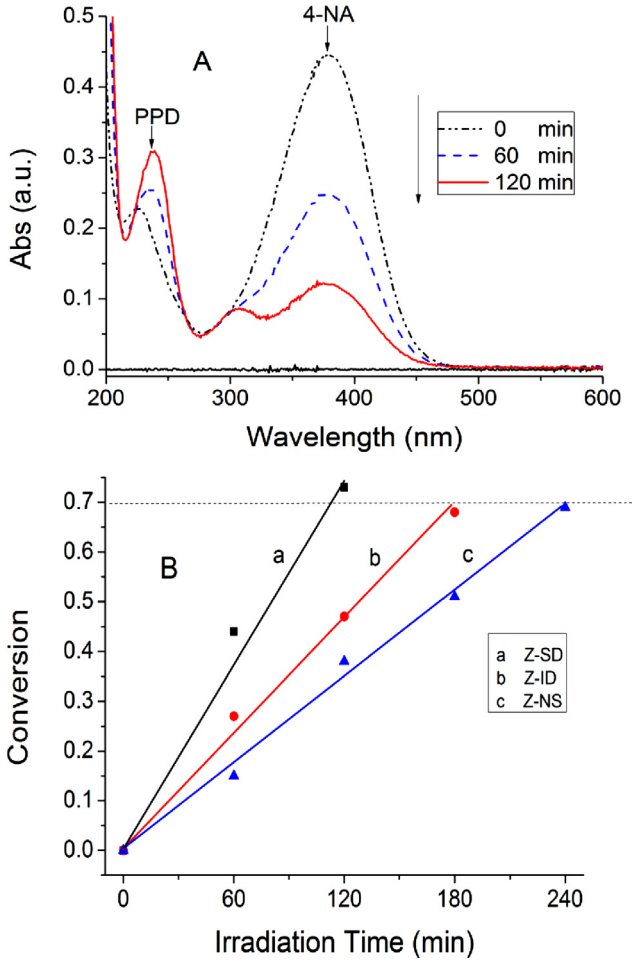


**Fig. 8.** Photocatalytic reduction of 4-NA over ZnO films: (A) UV–vis absorption variations of 4-NA and PPD over SD ZnO films; (B) Comparison of reduction capabilities of different ZnO films.

### 3.4. Promotion of photocatalytic activity by defects

Differences of performance of zinc oxide films in photocatalytic reactions mentioned above strongly suggest that defects act as decisive part in the activity. XPS results have confirmed the existence of defects created by CPT on SD films. Nevertheless, XPS cannot reveal the state of inner defects due to its limited detection depth. Thus, ESR, another powerful technique for analyzing defects (paramagnetic species), was further carried out to determine inner layer defective sites. Shown in Fig. 9 is the result of ESR measurement. Signal at $g = 2.003$ is commonly attributed to an unpaired electron trapped on an oxygen vacancy site [17,19,27]. Another high field signal at $g = 1.96$, sometimes was also attributed to oxygen vacancy, has been proved to relate to $Zn_i$ or other shallow donor impurities by Ischenko and co-workers [17]. However, since no impurities were detected by EDX (see Figure S4), this signal can be attributed to $Zn_i$ only. Apparently, densities of both oxygen vacancy and $Zn_i$ increased after CPT.

In common sense, semiconductor photocatalysts irradiated by light with appropriate wavelength can subsequently generate $e^-$–$h^+$ pairs. These charge carriers will either transfer across the interface to react with acceptors/donors or get trapped by various metastable defects. More likely, a large quantity of the $e^-$–$h^+$ pairs would recombine [37], and eventually annihilate. Therefore, competition among recombination, trapping, and transfer of the photo-generated charge carriers determines the overall quantum efficiency and further affect the photocatalytic activity. On the other hand, light absorbance of the material also plays crucial role over the performance of photocatalyst. To inspect the effect of defects on light absorption, we tested the UV–vis DRS of different films. The result (see Figure S5) shows that the light absorption spectra hardly changed despite the CPT process, which indicates that only local state defects were created [18]. In the present systems, "empty" oxygen site ($V_o^{2+}$) can trap either one ($V_o^+$) or two ($V_o^0$) electrons [17] and hence can promote the separation of $e^-$–$h^+$ pairs. Besides, both oxygen vacancies ($V_o^+$, $V_o^0$) and zinc interstitials ($Zn_i^0$, $Zn_i^+$) are electron donors and are considered to enhance donor density. The increased donor density can improve charge transport and shift Fermi level toward the conduction band, hence facilitate the charge separation at the semiconductor/electrolyte interface [42,43]. We deduce that the enhanced charge separation and transportation are the main promotion factors for defective ZnO samples.

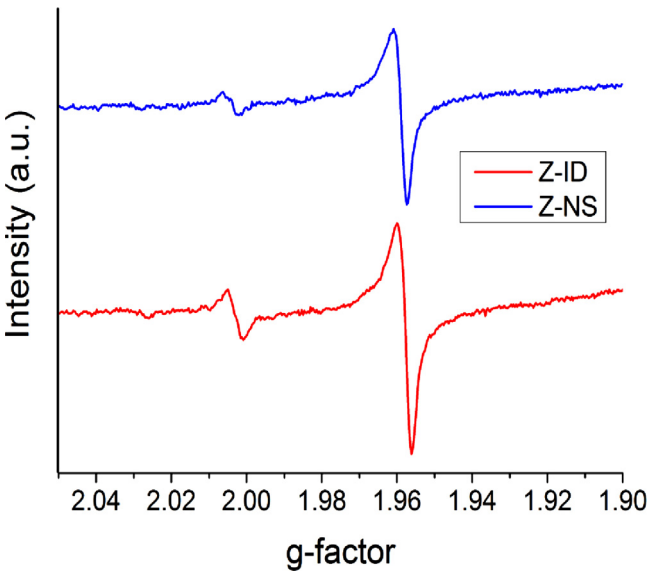


**Fig. 9.** Room-temperature ESR spectra of ID and NS ZnO.

To verify our hypothesis, electrochemical analyses, including EIS and Mott–Schottky plots, were carried out. The EIS spectra under 365 nm light irradiation are shown in Fig. 10. The radius of the

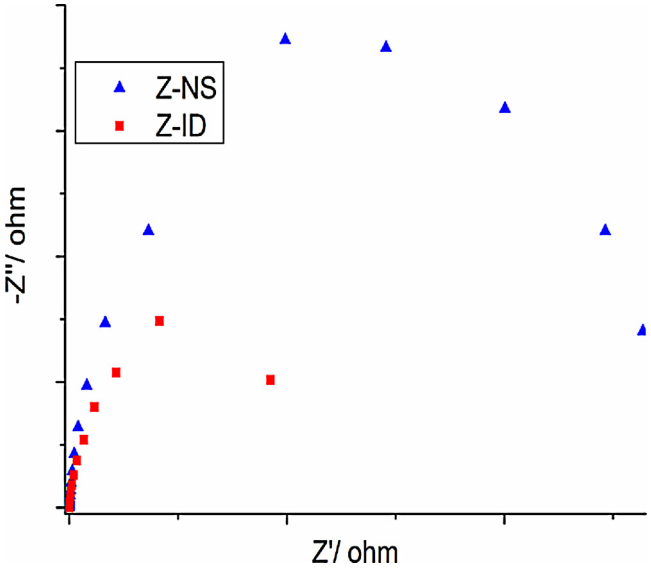


**Fig. 10.** The EIS of FTO/NS and FTO/ID ZnO film electrodes with an applied bias potential of 0.5 V under UV light irradiation.

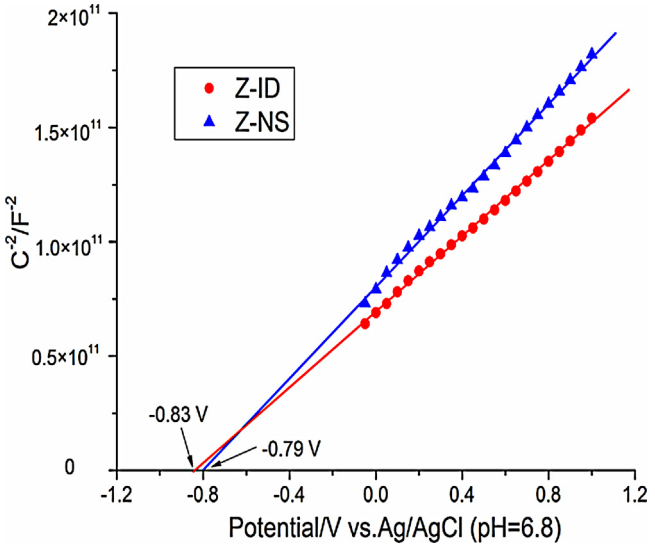


**Fig. 11.** Mott–Schotty plots of NS and ID ZnO films.

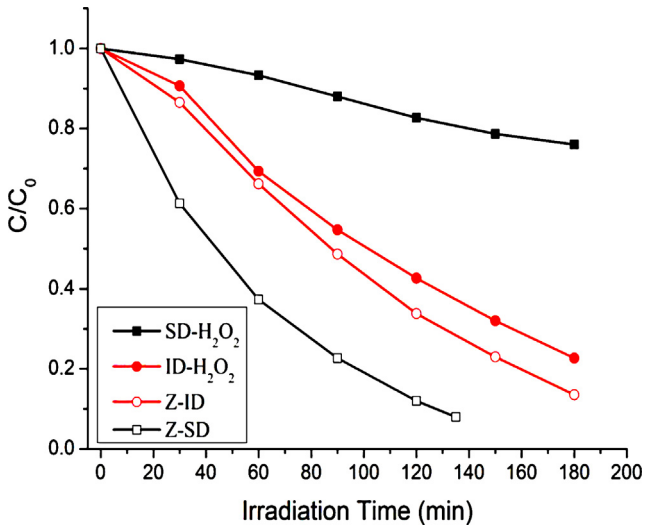


**Fig. 12.** Performance of SD and ID ZnO films before and after $H_2O_2$ treatment in photocatalytic degradation of MO under UV light.

arc on the Nynquist plot reflects reaction rate occurring at the surface of the electrode [44,45]. Obviously, the arc radius of FTO/Z-ID electrode is smaller than that of the FTO/Z-NS, which means a more effective separation of photoexcited $e^-$–$h^+$ pairs and that faster interfacial charge transfer had occurred [44]. Besides, the Mott–Schottky plots in Fig. 11 reveal a slight shift (0.04 V) toward negative potential, denoting upward shift of the Fermi level after CPT. Additionally, the smaller slope of Z-ID compared to Z-NS's also suggests an increase of donors [43]. The electrochemical measurements therefore confirm our postulation, that is, both $V_o$ and $Zn_i$ contribute to donor density and thus good transportation together with separation of $e^-$–$h^+$ pairs are achieved. As a consequence, the total photocatalytic activity is remarkably improved.

### 3.5. Stability of interfacial defect

As mentioned above, defect is metastable state and readily to be repaired. This is especially serious for defect located at surface of photocatalysts because it may be oxidized in air and is even susceptible to dissolved oxygen in water [19,24]. Moreover, surface defect, as active site, may be easily deactivated by reaction intermediates. Therefore, stabilization of defect is commonly concerned [23,26,46]. Investigations by other authors [25,26] together with our previous work [22] have demonstrated that intimal defect could promote photocatalytic activity and be protected in reaction process. To testify the stability of the intimal defect in ZnO, we immersed the newly prepared Z-ID and Z-SD films into 3 wt% $H_2O_2$ solution, a well-known oxidant, for 5 min followed by drying at 393 K in air for 30 min, and then tested their performance in degradation of MO. Displayed in Fig. 12 is the results of decomposition process under 365 nm irradiation. For the sake of comparison, original defective ZnO samples are also shown. After treatment by $H_2O_2$, significant deterioration of photocatalytic activity was observed for Z-SD films, indicating most defects on the surface were immediately repaired. In contrast, defects in the interlayer showed good stability. Moreover, the ESR spectra of Z-SD and Z-ID samples after treatment by $H_2O_2$ solution (see Figure S6) further confirm that more $V_o$ sites are repaired in Z-SD films. It is interesting to found that the zinc interstitials are sharply reduced even though the detailed process is yet to be known. Nevertheless, the comparison evidently suggests that outerlayer can effectively protect intimal defects and those active sites in interlayer can almost undergo high oxidative circumstance, which is of significance for practical use.

### 3.6. Dominance of interlayer defect

Since defect can efficaciously modulate performance of photocatalysts and be protected by outerlayer, then it occurs to us about the defects' dominance that could enhance the activity. Herein, dip-coating method well facilitated the intention as thickness of the film can be easily controlled through changing drawing speed [47]. Generally, in hydrophilic sol, the higher the withdrawal speed is, the thicker the film is [48]. We keep inner layer with the same thickness by controlling speed at 20 mm/min, then CPT were carried out on all films under identical conditions and eventually outerlayers were coated with different drawing speed. These films marked with their corresponding speed were further tested by photocatalytic decomposition of MO. For reference, equivalent films without CPT were also performed and the results are illustrated in Fig. 13. Promisingly, intimal defects are indeed able to promote photocatalytic reactivity with their location as deep as certain thickness corresponding to the drawing speed even at 100 mm/min. It is notable that thicker film is unbeneficial for degradation efficiency since the photocatalytic reaction occurred only on the surface of catalyst and charge carriers may recombine in a longer transfer route. However, our

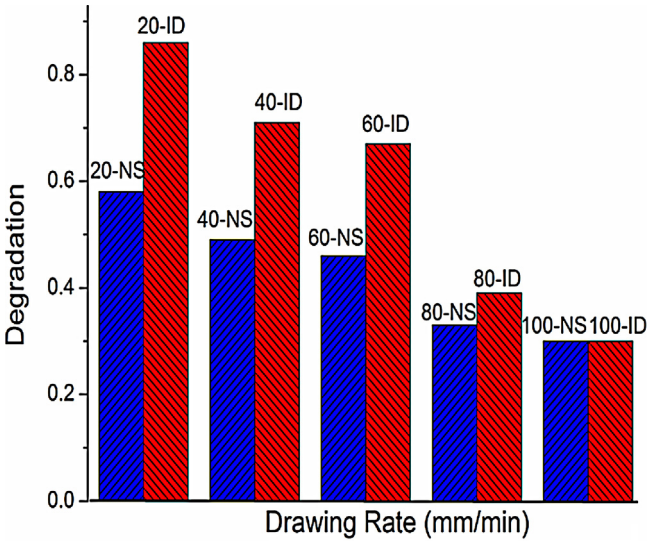


**Fig. 13.** Effect of defects in ZnO films with different thickness.

work demonstrates that intimal defects can, in some degree, affect activity of photocatalyst in the present systems. More importantly, the exact definition of surface/subsurface and bulk in still unknown, the present study may provide a new insight into this issue.

## 4. Conclusions

In summary, we successfully introduced defects into ZnO bilayer films by CPT technique. XPS and ESR demonstrated that the detected defective species were oxygen vacancies and interstitial zinc atoms. These defects remarkably promoted the photocatalytic activity of ZnO films in photodegradation of MO and 4-CP, with the main ROS being hydroxyl radicals. Besides, reduction capability of 4-NA to PPD was also enhanced by the defects. Further investigation revealed that both $V_o$ and $Zn_i$ increased donor density hence shifted Fermi level toward the conduction band. As a consequence, good transportation and separation of photo-excited charge carriers were achieved, and thus seen the improvement of photocatalytic performance. Defects in the interface, which could even almost survive $H_2O_2$ treatment, were quite stable and could promote degradation activity with their location as deep as certain thickness corresponding to the drawing speed at 100 mm/min in present system. It is expected that our study can provide a new insight into the role of defects over photocatalytic activity.

## Acknowledgments

The work is supported by National Natural Science Foundation of China (21173046, 21033003, 20977016, J1103303), National Basic Research Program of China (973 Program: 2010CB234604 and 2013CB632405) and Program for Changjiang Scholars and Innovative Research Team in University (PCSIRT0818).

## Appendix A. Supplementary data

Supplementary data associated with this article can be found, in the online version, at http://dx.doi.org/10.1016/j.apcatb.2013.05.055.

## References

[1] Z.L. Wang, J. Song, Science 312 (2006) 242.
[2] M.H. Huang, S. Mao, H. Feick, et al., Science 292 (2001) 1897–1899.
[3] A. Tsukazaki, A. Ohtomo, T. Onuma, et al., Nature Materials 4 (2005) 42–46.
[4] T. Shido, Y. Iwasawa, Journal of Catalysis 192 (1991) 343–355.
[5] T.J. Kuo, C.N. Lin, C.L. Kuo, M.H. Huang, Chemistry of Materials 19 (2007) 5143–5147.
[6] J. Wang, P. Liu, X. Fu, Z. Li, W. Han, X. Wang, Langmuir 25 (2009) 1218–1223.
[7] Y. Li, W. Xie, X. Hu, G.g. Shen, X. Zhou, Y. Xiang, X. Zhao, P. Fang, Langmuir 26 (2010) 591–597.
[8] A. Akyol, H.C. Yatmaz, M. Bayramoglu, Applied Catalysis B: Environmental 54 (2004) 19–24.
[9] A. Steinfeld, International Journal of Hydrogen Energy 27 (2002) 611–619.
[10] M.L. Cubeiro, J.L.G. Fierro, Journal of Catalysis 179 (1998) 150–162.
[11] Y. Li, X. Zhou, X. Hu, X. Zhao, P. Fang, Journal of Physical Chemistry C 113 (2009) 16188–16192.
[12] S.S. Warule, N.S. Chaudhari, B.B. Kale, M.A. More, CrystEngComm 11 (2009) 2776–2783.
[13] H.R. Liu, G.X. Shao, J.F. Zhao, Z.X. Zhang, Y. Zhang, J. Liang, X.G. Liu, H.S. Jia, B.S. Xu, Journal of Physical Chemistry C116 (2012) 16182–16190.
[14] Y. Wang, Sh Li, H. Shi, K. Yu, Nanoscale 4 (2012) 7817–7824.
[15] Y. Zheng, C. Chen, Y. Zhan, X. Lin, Q. Zheng, K. Wei, J. Zhu, Y. Zhu, Inorganic Chemistry 46 (2007) 6675–6682.
[16] M.Y. Guo, A.M.C. Ng, F. Liu, A.B. Djurisic, W.K. Chan, H. Su, K.S. Wong, Journal of Physical Chemistry C 115 (2011) 11095–11101.
[17] V. Ischenko, S. Polarz, D. Grote, V. Stavarache, K. Fink, M. Driess, Advanced Functional Materials 15 (2005) 1945–1954.
[18] I. Justicia, P. Ordejón, G. Canto, J.L. Mozos, J. Fraxedas, G.A. Battiston, R. Gerbasi, A. Figueras, Advanced Materials 14 (2002) 1399–1402.
[19] J. Zhuang, S. Weng, W. Dai, P. Liu, Q. Liu, Journal of Physical Chemistry C 116 (2012) 25354–25361.
[20] M. Kong, Y. Li, X. Chen, T. Tian, P. Fang, F. Zheng, X. Zhao, Journal of the American Chemical Society 133 (2011) 16414–16417.
[21] C.A. Paez, D. Poelman, J.P. Pirard, B. Heinrichs, Applied Catalysis B: Environmental 94 (2010) 263–271.
[22] J. Zhuang, W. Dai, Q. Tian, Z. Li, L. Xie, J. Wang, P. Liu, Langmuir 26 (2010) 9686–9694.
[23] A. Danon, K. Bhattacharyya, B.K. Vijayan, J. Lu, D.J. Sauter, K.A. Gray, P.C. Stair, E. Weitz, ACS Catalysis 2 (2012) 45–49.
[24] B.K. Na, A.B. Walters, M.A. Vannice, Journal of Catalysis 140 (1993) 585–600.
[25] X. Chen, L. Liu, P.Y. Yu, S.S. Mao, Science 331 (2011) 746–750.
[26] A. Naldoni, M. Allieta, S. Santangelo, M. Marelli, F. Fabbri, S. Cappelli, C.L. Bianchi, R. Psaro, V.D. Santo, Journal of the American Chemical Society 134 (2012) 7600–7603.
[27] H. Liu, H.T. Ma, X.Z. Li, W.Z. Li, M. Wu, X.H. Bao, Chemosphere 50 (2003) 39–46.
[28] N. Wu, M. Lee, Z. Pon, J. Hsu, Journal of Photochemistry and Photobiology A: Chemistry 163 (2004) 277–280.
[29] E. Lira, S. Wendt, P. Huo, J.O. Hansen, R. Streber, S. Porsgaard, Y. Wei, R. Bechstein, E. Laegsgaard, F. Besenbacher, Journal of the American Chemical Society 133 (2011) 6529–6532.
[30] M.N. Islam, T.B. Ghosh, K.L. Chopra, H.N. Acharya, Thin Solid Films 280 (1996) 20–25.
[31] M. Chen, X. Wang, Y.H. Yu, Z.L. Pei, X.D. Bai, C. Sun, R.F. Huang, L.S. Wen, Applied Surface Science 158 (2000) 134–140.
[32] L. Jing, Z. Xu, X. Sun, J. Shang, W. Cai, Applied Surface Science 108 (2001) 308–314.
[33] P.T. Hsieh, Y.C. Chen, K.S. Kao, C.M. Wang, Applied Physics A 90 (2008) 317–321.
[34] A. Fujishima, X.T. Zhang, D.A. Tryk, Surface Science Reports 63 (2008) 515–582.
[35] S. Zhu, S. Liang, Q. Gu, L. Xie, J. Wang, Z. Ding, P. Liu, Applied Catalysis B: Environmental 119–120 (2012) 146–155.
[36] A. Amine-Khodja, A. Boulkamh, C. Richard, Applied Catalysis B: Environmental 59 (2005) 147–154.
[37] M.R. Hoffmann, S.T. Martin, W. Choi, D.W. Bahnemann, Chemical Reviews 95 (1995) 69–96.
[38] L. Spanhel, H. Weller, A. Henglein, Journal of the American Chemical Society 109 (1987) 6632–6635.
[39] W. Wu, G. Liu, S. Liang, Y. Chen, L. Shen, H. Zheng, R. Yuan, Y. Hou, L. Wu, Journal of Catalysis 290 (2012) 13–17.
[40] W. Wu, L. Wen, L. Shen, R. Liang, R. Yuan, L. Wu, Applied Catalysis B: Environmental 130–131 (2013) 163–167.
[41] J.L. Ferry, W.H. Glaze, Langmuir 14 (1998) 3551–3555.
[42] D.C. Cronemeyer, Physical Review 113 (1959) 1222–1226.
[43] G. Wang, H. Wang, Y. Ling, Y. Tang, X. Yang, R.C. Fitzmorris, C. Wang, J.Z. Zhang, Y. Li, Nano Letters 11 (2011) 3026–3033.
[44] H. Zhang, R. Zong, Y. Zhu, Journal of Physical Chemistry C 113 (2009) 4605–4611.
[45] W.H. Leng, Z. Zhang, J.Q. Zhang, C.N. Cao, Journal of Physical Chemistry B 109 (2005) 15008–15023.
[46] F. Zuo, L. Wang, T. Wu, Z. Zhang, D. Borchardt, P. Feng, Journal of the American Chemical Society 132 (2010) 11856–11857.
[47] M. Faustini, B. Louis, P.A. Albouy, M. Kuemmel, D. Grosso, Journal of Physical Chemistry C 114 (2010) 7637–7645.
[48] H. Segawa, S. Adachi, Y. Arai, K. Yoshida, Journal of the American Ceramic Society 86 (2003) 761–764.